RSC Advances

PAPER

View Article Online
View Journal | View Issue

Cite this: *RSC Adv.*, 2014, **4**, 35609

MoS_2 nanosheet production by the direct exfoliation of molybdenite minerals from several type-localities†

Nicky Savjani,[a] Edward A. Lewis,[b] Richard A. D. Pattrick,[c] Sarah J. Haigh[b] and Paul O'Brien*[ab]

Received 30th April 2014
Accepted 6th August 2014

DOI: 10.1039/c4ra03982c

www.rsc.org/advances

Samples of the mineral molybdenite from three classic molybdenum mining localities were examined as a potential source of molybdenum disulfide (MoS_2) nanosheets. In all cases, ultrasonication-promoted exfoliation of these samples in *N*-methylpyrrolidone (NMP) was found to produce MoS_2 as dispersed nanosheets with lateral sizes in the range of 200–600 nm and thicknesses between 1 and 10 atomic trilayers. The MoS_2 nanosheets obtained were found to be highly crystalline and largely defect-free, but tend to contain small amounts of aggregates on their surfaces. The exfoliated MoS_2 dispersions were characterised by UV-Vis spectroscopy, Raman spectroscopy, scanning electron microscopy (SEM), (scanning) transmission electron microscopy ((S)TEM) and energy dispersive X-ray (EDX) spectroscopy. This work raises the possibility that mined, unrefined minerals could be a source of low-dimensional MoS_2.

Introduction

Atomically thin graphene exhibits exceptional electronic, optical and mechanical properties.[1] Since graphenes' initial discovery[2] there has been an explosion of interest[3] in other 2D materials, leading to the exploration of graphene analogues such as the family of transition metal dichalcogenides, or TMDCs (MX_2; *e.g.* M = Mo, W and X = S, Se, Te). TMDCs all display similar layered-graphitic superstructures.[4] These structures are comprised of a layer of transition metal atoms coordinated by two layers of close-packed chalcogen atoms, held together by strong covalent bonds. In the bulk material, these sheets are bound together by weak van der Waals forces, just as in graphite.[5] Of these 2D-TMDC materials, MoS_2 nanosheets are potentially a useful semiconducting component in a series of devices.[6,7] In addition, molybdenum disulfide exhibits considerable anisotropy, giving rise to novel electronic, optical, structural and mechanical properties in its 2D form (2D-MoS_2). Due to these properties 2D-MoS_2 has been shown to be a suitable material for inclusion in a myriad of potential applications that includes photochemical sensors,[8,9] optoelectronics,[10,11] bioimaging,[12,13] catalysis,[14,15] solid-state lubricants,[16] and energy storage.[17,18]

In many cases, laboratory-scale 2D-MoS_2 production is based on liquid exfoliation of molybdenum(IV) sulfide powder.[19] The powder is refined from natural MoS_2, molybdenite, which is mined in numerous pan-global locations and purified by comminution, flotation and leaching.[20,21] In the years 2006–2011, demand has surged to 264,000 tonnes per year of molybdenum metal, an increase of 25%.[22,23] The demand of the mineral is driven by metallurgical, green- and now nanomaterial-based applications.[20]

Herein we discuss the feasibility of MoS_2 nanosheet production by exfoliation of molybdenite ores, as exemplified by samples obtained from three locations (Queensland AUS [QL], New South Wales AUS [NSW] and Telemark NOR [TM]). The crystalline molybdenite samples were obtained untreated from the selected minerals (see Table S1† for purity analysis). The potential to obtain MoS_2 nanosheet from these sources by employing the Coleman method of MoS_2 exfoliation is detailed in this report.[24,25] The nanomaterials produced have been subject to a comparison of exfoliation efficiency, as well as compositional and structural features, relative to the nanosheets produced from MoS_2 powder documented in the literature.[24]

Results and discussion

50 mL solutions of *N*-methylpyrrolidone (NMP) containing flakes of the selected molybdenite (375 mg, 7.5 mg mL^{-1} concentrations) were bath ultrasonicated for 48 hours, with aliquots obtained at various time intervals. Unexfoliated

[a]School of Chemistry, The University of Manchester, Oxford Road, M13 9PL, UK. E-mail: paul.o'brien@manchester.ac.uk; Tel: +44 (0)161 2754652
[b]School of Materials, The University of Manchester, Oxford Road, M13 9PL, UK
[c]School of Earth, Atmospheric and Environmental Sciences, The University of Manchester, Oxford Road, Manchester, M13 9PL, UK

† Electronic supplementary information (ESI) available: UV-Vis, Raman, SEM, HAADF STEM and EDX data of the nanosheets produced from QL, NSW and TM-sourced materials. See DOI: 10.1039/c4ra03982c

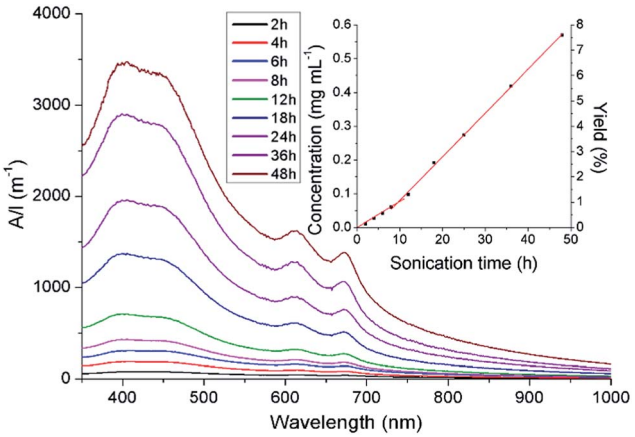

Fig. 1 UV-Vis absorption spectrum stack plot of MoS_2 dispersions obtained from the QL concentrate at different time intervals. The inserted graph shows the concentration of the MoS_2 dispersion from the QL concentrate, relative to sonication time.

material was removed from the aliquots by centrifugation (45 minutes at 1500 rpm). UV-visible spectra of the supernatants showed two peaks with maxima at 628 and 674 nm, attributed to the characteristic A and B direct excitonic transitions of MoS_2 respectively (Fig. 1, S1a and S2a†).[24]

The UV-Vis data was modified to remove the background noise associated with the scattering exponent of the MoS_2 nanosheets.[24] The intensity of the feature at *ca.* 674 nm was then used as a spectroscopic handle to estimate the concentrations of the MoS_2 dispersions produced.[25] The final concentrations of the exfoliates were found to be 0.57, 0.42 and 0.84 mg mL^{-1}, from QL, NSW and TM precursors, respectively. These values obtained are considerably lower than the concentration of 1.79 mg mL^{-1} produced from the exfoliation of bulk-MoS_2 powder, which was run alongside the molybdenite samples. In all cases, plots of concentration *versus* sonication times (insert in Fig. 1, S1b and S2b†) reveal at least two kinetic regimes of MoS_2 nanosheet production, as the exfoliation rates (k_{exf}) in the initial 12 hours of sonication are noticeably slower than those observed after this period. Using the values of k_{exf} obtained after this initial 12 hour period, it was clear to see the selection of the concentrate results in different exfoliation rates (k_{exf} between 9.4 and 20.7 μg mL^{-1} h^{-1}; Table S2†). The rates of exfoliation were also found to be significantly lower than those observed for the exfoliation of bulk-MoS_2 powder (37.1 μg mL^{-1} h^{-1}). Stability investigations show that there is a very small (<4%) reduction in the intensity of the A and B bands over a period of 4 weeks; indicating that the dispersions are highly stable (Fig. S3†).

In all molybdenite sources, both large flakes from the crystalline aggregates and the exfoliated nanosheets exhibit two Raman peaks that correspond to the A_{1g} and E_{2g} modes (Fig. 2a–c). These peaks are known to exhibit a well-defined dependence on layer *z*-thickness and thus can be used as a way of estimating nanosheet thickness.[26] All of our exfoliations gave few-layer MoS_2 nanosheets as the predominant product. Nanosheets from the TM dispersion showed the two modes separated by 19 cm^{-1}, similar to the peak separation observed for single-layered MoS_2 nanosheets exfoliated from MoS_2 powder.[24,27] It was expected that exfoliation of the QL and NSW concentrates also produced single-layered 2D-MoS_2, however, these were not

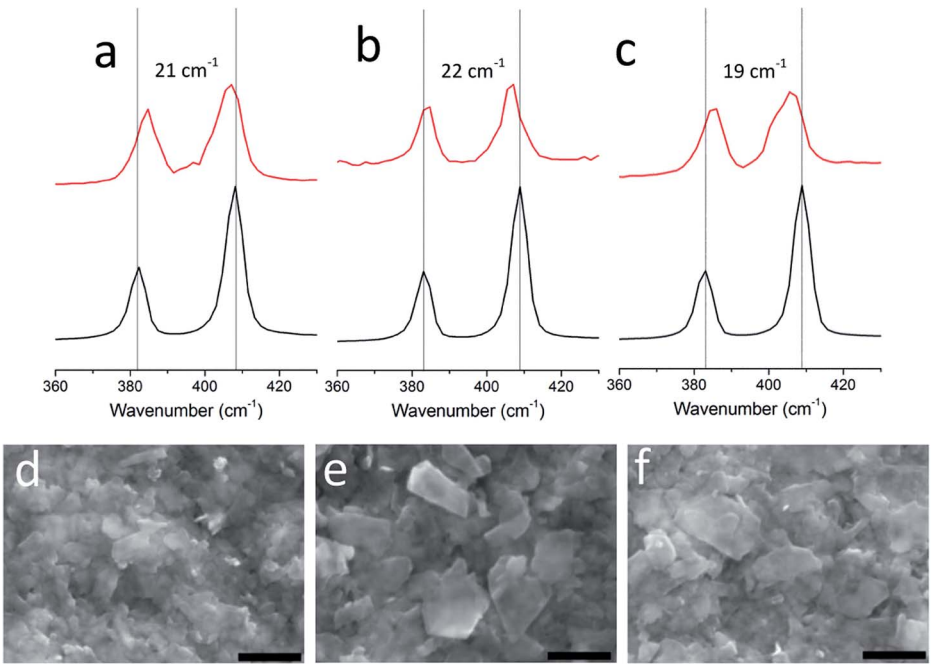

Fig. 2 (a–c) Selected range (360–430 cm^{-1}) Raman spectra for QL-, NSW- and TM-sourced materials, respectively. In each spectra, a comparison between the bulk material (black) and the exfoliated nanosheets (red, separation of peaks = 26 cm^{-1}) can be made. (d–f) SEM images of the MoS_2 thin films on a PVDF membrane from the (d) QL-, (e) NSW- and (f) TM-sourced dispersions. Scale bars set at 500 nm.

detected in the Raman spectra obtained from either exfoliated sample, presumably due to the smaller lateral dimensions of the nanosheets. Statistical analysis (sample size = 50, Fig. S4†) of randomly selected flakes indicates that more than 80% of the flakes dispersed contain less that 6 stacked monolayers. The remaining areas were covered with thicker material whose thickness could not be determined by Raman spectropscopy.[26]

Membrane-supported thin films of MoS_2 nanosheets were prepared from the QL, NSW and TM dispersions by vacuum filtration[24,28] and imaged by scanning electron microscopy (SEM). All films produced were found to have similar surface morphology (Fig. 2d–f and S5†); the surface of the films consist of partially-stacked 2D-nanosheets with lateral dimensions between 200–600 nm.

Nanosheets were deposited onto lacey carbon grids for (scanning) transmission electron microscope ((S)TEM) imaging. The resulting HAADF STEM images (Fig. 3) and TEM images (Fig. S6†) show faceted morphologies and a range of irregular shapes. The lateral dimensions of the nanosheets ranged from 200 nm to greater than 1 μm. Selected area diffraction (SAED) patterns (Fig. S6†) confirmed that in all samples, most flakes consisted of single crystals and that all of the flakes had the expected hexagonal crystal structure. Atomic resolution, high-angle annular dark-field (HAADF) STEM imaging (Fig. 2 and S7†) confirmed that all flakes were highly crystalline and largely defect-free. The edge structure of flakes observed in high magnification HAADF STEM images can be used to estimate flake thickness.[24] The majority of the flakes were found to be 1–10 layers thick, although flake thicknesses varied for different areas within individual flakes.

Energy-dispersive X-ray (EDX) spectroscopy measurements, performed in the SEM and STEM, were used to obtain compositional information from both the thin films and individual flakes. Quantitative analysis gave the expected Mo : S ratio of 1 : 2 in all cases. STEM-EDX mapping revealed calcium rich regions in all samples, believed to be nanometre scale calcium carbonate aggregates on the flake's surface (Fig. S8–11†). Nanosheets prepared from the NSW source showed significantly more calcium contamination than nanosheets made from the other sources. SEM-EDX analyses did not show any significant quantities of calcium, but did detect other elements: all samples were found to contain non-negligible amounts of iron, in addition to bismuth found in QL and NSW thin films (Fig. S8–10†).

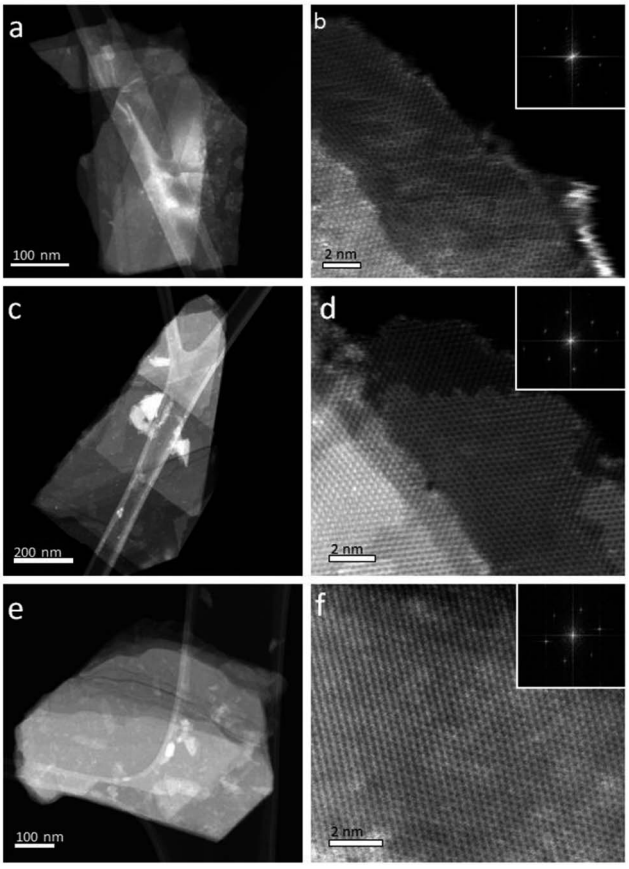

Fig. 3 HAADF STEM images of a representative selection of nanosheets obtained from QL (a and b), NSW (c and d) and TM-sources (e and f). Fourier transforms for each of the lattice resolution images are inset for (b), (d) and (f) and illustrate the expected single crystal lattice symmetry.

Conclusions

We have shown that untreated molybdenite mineral samples can be used as a precursor for exfoliation to produce few-layered MoS_2 nanosheets that are highly crystalline, and largely defect-free, with small amounts of aggregates on the surface of the sheets. The selection of molybdenite source from various locations worldwide appears to have little effect on the purity or crystallinity of the nanosheets produced. In addition thin films comprised of stacked MoS_2 nanosheets have been produced using a simple filtration method. The relatively high purity of the nanosheets and thin films produced by the methodology described herein gives hope that a cost-effective approach for the production of MoS_2 for components in electrical circuitry using relatively unrefined material is possible. The electronic properties of the nanosheets produced are currently the subject of further work.

Experimental section

Background information

The molybdenite aggregates were obtained from selected molybdenite-containing mines: Toowong, Queensland (AUS); Kingsgate, New South Wales (AUS) and Siljord, Telemark (NOR). Compositional analysis of the aggregates were obtained by a Chemeca Camebax SX100 microsonde Electron Probe Micro-Analyser (EPMA), running a 20 nA beam at 20 keV with a 1.5 μm spot size on polished sections. The measurements were compared to elemental standards: Ni, Co, Fe, Re, W and Bi metals, MoS_2, $CuFeS_2$, ZnS and ZnSe. Molybdenum(IV) sulfide powder and *N*-methylpyrrolidone (NMP) were purchased from Sigma-Aldrich, which were used as supplied.

The dispersions were prepared in a bench-top sonication bath (Elmasonic P 70H [HF power 820 W across four horns]).

Centrifugations were carried out using Centurion 822 series (up to 15 mL dispersions) and Jouan B4i (up to 50 mL dispersions) centrifuges. UV-Vis absorption spectroscopy was performed with an Agilent 8453 spectrometer using a 1 cm glass cuvette. Accurate dilutions of the MoS_2 dispersions in NMP were produced to obtain suitable UV-Vis spectra. The subsequent data was then analysed after modification (implementing the Beer–Lambert law) to represent the absorption intensities at the concentrations when the aliquots were first taken from the reaction.

Membrane-supported thin films of MoS_2 nanosheets suitable for Scanning Electron Microscopy (SEM) were produced by the dilution of 30 mL suspensions in isopropanol (270 mL), and filtration through a polyvinylidene fluoride membrane (PVDF, pore size 0.1 μm). The thin films were washed with isopropanol (3 × 50 mL) before drying in a vacuum chamber for 12 hours at ambient temperature. The thin films are carbon-coated using a Gatan Model 682 Precision Etching coating system before carrying out SEM and EDX analyses by the use of Philips XL 30FEG scanning electron microscope and a DX4 detector.

Raman spectra were acquired on a Renishaw 1000 system, with a solid state 50 mW 514.5 nm laser. The laser beam was focused onto the MoS_2 sample by a 100× objective lens. The scattered signal was detected by an air cooled CCD detector. Samples were prepared by dilution of the NMP dispersions with ethanol (1 : 40 v/v), before deposition onto a 300 nm SiO_2/Si substrate and drying under ambient conditions over 48 hours.

Samples were prepared for transmission electron microscope (TEM) imaging by drop casting a dilute solution of the MoS_2 dispersions (1% solution in EtOH) onto holey carbon support films which were then washed with ethanol and air dried. Flake size and shape was assessed using low magnification bright field TEM in a Philips CM20 and a FEI Tecnai F20, both microscopes used a LaB_6 electron source and were operated at 200 kV. High angle annular dark field (HAADF) scanning transmission electron microscope (STEM) imaging was performed using a probe side aberration corrected FEI Titan G2 operated at 200 kV. For HAADF imaging a convergence angle of 26 mrad, a HAADF inner angle of 52 mrad, and a probe current of ~200 pA were employed. Energy dispersive X-ray (EDX) spectroscopy was performed in the Titan using a Super-X EDX detector with a solid angle of collection of 0.7 s rad. EDX quantification was performed using Brüker Esprit software, where the bremsstrahlung background was subtracted, peaks deconvoluted, and quantification performed using the Cliff–Lorimer approach. Fe, Cu, Zr, and C counts were known to originate from the microscope (Fe and Zr) and support film (Cu and C), so these elements were included in the deconvolution procedure but excluded from the final quantification.

Purity of molybdenite aggregates

The molybdenite aggregates were analysed by Electron probe Microanalysis (EPMA) and found to be of high purities (>99.5%; Table S1†). The trace element populations are low (below detection limits in many analysis spots), nor were there any major substitution. Bi was detected in the sample from QL where Bi_2S_3 was an associated phase. The high standard deviations reveal the high variations. The Re and W do appear in several points in the analyses above detection and are probably real.

Synthesis of MoS_2 dispersions from the aggregates

In a 60 mL screw-cap glass jar, NMP (50 mL) was added to 375 mg of the chosen molybdenite aggregate (manually broken up into approx. 10 flakes) before suspending the sealed jars in an operational ultrasonic bath for 48 hours. For concentration determination, 3 mL aliquots of the dispersions were removed at selected time intervals and diluted in NMP (3 mL) within a 15 mL centrifuge tube. Each aliquot was left to settle overnight before centrifugation at 1500 rpm for 45 minutes. Two-thirds of the resulting supernatant was pipetted to provide a suspension of MoS_2 nanosheets in NMP (note: at 50% of its initial concentration). After 48 hours the dispersions that remained in the reaction vessels (approx. 25 mL) were decanted into 50 mL centrifuge tubes containing 20 mL NMP and left to settle overnight. Centrifugation at 1500 rpm for 45 minutes followed by pipetting of 30 mL of the supernatant gave a suspension of MoS_2 nanosheets of suitable quantities for thin film production.

Acknowledgements

NS and POB thank to the Parker family for funding this work. EL thanks the Engineering and Physical Sciences Research Council (UK) and the North West Nanoscience Doctoral Training Centre (NOWNano DTC) for supporting his work. SJH thanks the Defence threat reduction agency for funding support. All authors acknowledge Dr Christopher Wilkins and David Lewis for their input in SEM.

Notes and references

1 R. S. Edwards and K. S. Coleman, *Nanoscale*, 2013, **5**, 38–51.
2 K. S. Novoselov, A. K. Geim, S. V. Morozov, D. Jiang, Y. Zhang, S. V. Dubonos, I. V. Grigorieva and A. A. Firsov, *Science*, 2004, **306**, 666–669.
3 A. H. C. Neto and K. Novoselov, *Mater. Express*, 2011, **1**, 10–17.
4 J. A. Wilson and A. D. Yoffe, *Adv. Phys.*, 1969, **18**, 193–335.
5 X. Huang, Z. Zeng and H. Zhang, *Chem. Soc. Rev.*, 2013, **42**, 1934–1946.
6 J. Pu, Y. Zhang, Y. Wada, J. T.-W. Wang, L.-J. Li, Y. Iwasa and T. Takenobu, *Appl. Phys. Lett.*, 2013, **103**, 023505.
7 K. Choi, Y. T. Lee, S.-W. Min, H. S. Lee, T. Nam, H. Kim and S. Im, *J. Mater. Chem. C*, 2013, **1**, 7803–7807.
8 B. Liu, L. Chen, G. Liu, A. N. Abbas, M. Fathi and C. Zhou, *ACS Nano*, 2014, **8**, 5304–5314.
9 F. K. Perkins, A. L. Friedman, E. Cobas, P. M. Campbell, G. G. Jernigan and B. T. Jonker, *Nano Lett.*, 2013, **13**, 668–673.
10 G. Cunningham, U. Khan, C. Backes, D. Hanlon, D. McCloskey, J. F. Donegan and J. N. Coleman, *J. Mater. Chem. C*, 2013, **1**, 6899–6904.

11 G. Eda and S. A. Maier, *ACS Nano*, 2013, **7**, 5660–5665.
12 J. Huang, Z. Dong, Y. Li, J. Li, W. Tang, H. Yang, J. Wang, Y. Bao, J. Jin and R. Li, *Mater. Res. Bull.*, 2013, **48**, 4544–4547.
13 V. Stengl and J. Henych, *Nanoscale*, 2013, **5**, 3387–3394.
14 D. Y. Chung, S.-K. Park, Y.-H. Chung, S.-H. Yu, D.-H. Lim, N. Jung, H. C. Ham, H.-Y. Park, Y. Piao, S. J. Yoo and Y.-E. Sung, *Nanoscale*, 2014, **6**, 2131–2136.
15 R. J. Young, in *Proceedings 22nd Saudi Japan Annual Symposium; Catalysts in Petroleum Refining & Petrochemicals*, Curran Associates, Inc., Saudi Arabia, 2012.
16 Z. Wu, D. Wang, Y. Wang and A. Sun, *Adv. Eng. Mater.*, 2010, **12**, 534–538.
17 K.-J. Huang, L. Wang, Y.-J. Liu, Y.-M. Liu, H.-B. Wang, T. Gan and L.-L. Wang, *Int. J. Hydrogen Energy*, 2013, **38**, 14027–14034.
18 S. Q. Liang, J. Zhou, J. Liu, A. Q. Pan, Y. Tang, T. Chen and G. Z. Fang, *CrystEngComm*, 2013, **15**, 4998–5002.
19 V. Nicolosi, M. Chhowalla, M. G. Kanatzidis, M. S. Strano and J. N. Coleman, *Science*, 2013, **340**, 1420.
20 R. F. Sebenik, A. R. Burkin, R. R. Dorfler, J. M. Laferty, G. Leichtfried, H. Meyer-Grünow, P. C. H. Mitchell, M. S. Vukasovich, D. A. Church, G. G. Van Riper, J. C. Gilliland and S. A. Thielke, in *Ullmann's Encyclopedia of Industrial Chemistry*, Wiley-VCH Verlag GmbH & Co. KGaA, 2000.
21 S. M. Bulatovic, D. M. Wyslouzil and C. Kant, *Miner. Eng.*, 1998, **11**, 313–331.
22 D. E. Polyak, *2011 Minerals Yearbook: Vol. I – Metals and Minerals*, Interior Dept., U.S. Geological Survey, Washington DC, 2012.
23 A. S. W. T. J. Brown, N. E. Idoine, R. A. Shaw, C. E. Wrighton, T. Bide, *British Geological Survey 2012: World Mineral Production 2006-10*, British Geological Survey, Keyworth, Nottingham, 2012.
24 J. N. Coleman, M. Lotya, A. O'Neill, S. D. Bergin, P. J. King, U. Khan, K. Young, A. Gaucher, S. De, R. J. Smith, I. V. Shvets, S. K. Arora, G. Stanton, H. Y. Kim, K. Lee, G. T. Kim, G. S. Duesberg, T. Hallam, J. J. Boland, J. J. Wang, J. F. Donegan, J. C. Grunlan, G. Moriarty, A. Shmeliov, R. J. Nicholls, J. M. Perkins, E. M. Grieveson, K. Theuwissen, D. W. McComb, P. D. Nellist and V. Nicolosi, *Science*, 2011, **331**, 568–571.
25 A. O'Neill, U. Khan and J. N. Coleman, *Chem. Mater.*, 2012, **24**, 2414–2421.
26 S. L. Li, H. Miyazaki, H. Song, H. Kuramochi, S. Nakaharai and K. Tsukagoshi, *ACS Nano*, 2012, **6**, 7381–7388.
27 Y. Yao, L. Tolentino, Z. Yang, X. Song, W. Zhang, Y. Chen and C.-p. Wong, *Adv. Funct. Mater.*, 2013, **23**, 3577–3583.
28 Y. Hernandez, V. Nicolosi, M. Lotya, F. M. Blighe, Z. Sun, S. De, I. T. McGovern, B. Holland, M. Byrne, Y. K. Gun'Ko, J. J. Boland, P. Niraj, G. Duesberg, S. Krishnamurthy, R. Goodhue, J. Hutchison, V. Scardaci, A. C. Ferrari and J. N. Coleman, *Nat. Nanotechnol.*, 2008, **3**, 563–568.